Scherler, D., Wulf, H., Gorelick, N. (2018): Global Assessment of Supraglacial Debris-Cover Extents. - *Geophysical Research Letters*, *45*, 21, pp. 11,798—11,805.

DOI: http://doi.org/10.1029/2018GL080158

Geophysical Research Letters

RESEARCH LETTER
10.1029/2018GL080158

Global Assessment of Supraglacial Debris-Cover Extents

Dirk Scherler[1,2], Hendrik Wulf[3], and Noel Gorelick[3,4]

[1]GFZ German Research Centre for Geosciences, Potsdam, Germany, [2]Institute of Geological Sciences, Freie Universität Berlin, Berlin, Germany, [3]Remote Sensing Laboratories, University of Zürich, Zürich, Switzerland, [4]Google Switzerland, Zurich, Switzerland

Key Points:
- We present new global data sets on supraglacial debris cover, based on Landsat 8 and Sentinel-2 satellite imagery
- Global debris cover (excluding the Greenland ice sheet and Antarctica) is ~4.4% by area, but heterogeneously distributed
- On a global scale, debris-cover fractions decrease with increasing glacier size

Supporting Information:
- Supporting Information S1

Correspondence to:
D. Scherler,
scherler@gfz-potsdam.de

Citation:
Scherler, D., Wulf, H., & Gorelick, N. (2018). Global assessment of supraglacial debris-cover extents. *Geophysical Research Letters*, *45*, 11,798–11,805. https://doi.org/10.1029/2018GL080158

Received 4 SEP 2018
Accepted 21 OCT 2018
Accepted article online 25 OCT 2018
Published online 8 NOV 2018

Abstract Rocky debris on glacier surfaces influences ice melt rates and the response of glaciers to climate change. However, scarce data on the extent and evolution of supraglacial debris cover have so far limited its inclusion in regional to global glacier models. Here we present global data sets of supraglacial debris-cover extents, based on Landsat 8 and Sentinel-2 optical satellite imagery. We find that about 4.4% (~26,000 km^2) of all glacier areas (excluding the Greenland ice sheet and Antarctica) are covered with debris, but that the distribution is heterogeneous. The largest debris-covered areas are located in high-mountain ranges, away from the poles. At a global scale, we find a negative scaling relationship between glacier size and percentage of debris. Therefore, the influence of debris cover on glacier mass balances is expected to increase in the future, as glaciers continue to shrink.

Plain Language Summary Most of the melting of land-terminating glaciers occurs at their surface. In mountainous regions, these ice surfaces are often partly covered by rocks and sediments (debris), which can amplify, or reduce, ice melt rates, depending on debris thickness. So far, however, debris cover is rarely taken into account in models of how glaciers respond to climate change. New global data sets of debris-cover extents, based on high-resolution satellite imagery, indicate that ~4.4% of all glacier surfaces (excluding the Greenland ice sheet and Antarctica) are covered with debris. Debris cover is particularly common in high and steep mountain ranges but is rare in low-relief landscapes, closer to the poles. Our findings provide a basis for including debris-cover effects in regional to global glacier models.

1. Introduction

Glaciers other than the ice sheets cover approximately 0.5% of the terrestrial land surface (Pfeffer et al., 2014), but their extent is shrinking due to ongoing climate change (Vaughan et al., 2013). Melting of land ice has the potential to significantly contribute to sea level rise and affect the availability of fresh water for drinking, irrigation, and hydropower (e.g., Huss & Hock, 2018). Assessing the consequences of glacier shrinking from local to global scales is thus an important task. Global-scale predictions of glacier evolution combine glacier mass balance models with assessments of present-day glacier geometry (e.g., Huss & Hock, 2015; Marzeion et al., 2012). The surfaces of mountain glaciers are frequently covered by supraglacial debris that can amplify or dampen ice melt rates, depending on its thickness (Østrem, 1959). The extent and thickness of supraglacial debris cover is likely a complex function of debris supply rates from ice-surrounding rock walls, its transport by the ice, and ice ablation that exposes englacial debris at the glacier surface (e.g., Kirkbride & Deline, 2013). Because all of these processes can vary with time, the extent and thickness of supraglacial debris cover are not constant but changes with time, too. Historical observations from the Mont Blanc massif, for example, indicate significant expansion of supraglacial debris cover over the last 150 years (Deline, 2005). However, similar observations are rare for most ice-covered regions on Earth (e.g., Herreid et al., 2015) and we currently lack observations to develop and test models of how debris-cover extents and thicknesses change with time.

Here we propose an approach to automatically map supraglacial debris cover from optical satellite images at a global scale. Our approach makes use of the cloud-computing platform Google Earth Engine (GEE; https://earthengine.google.com/) and exploits the large number of optical satellite images that are currently available. In this contribution, we present mapping results from Landsat 8 and Sentinel-2 images, with 30 and 10 m spatial resolution, respectively. In principle, our approach allows rapidly mapping changes in the distribution and extent of debris cover at any time period, for which suitable satellite imagery is available in GEE, such as the Landsat data sets (Gorelick et al., 2017). The goal of this contribution is twofold. First, we present our new automatic mapping approach and evaluate it by comparison with a recently published data set of

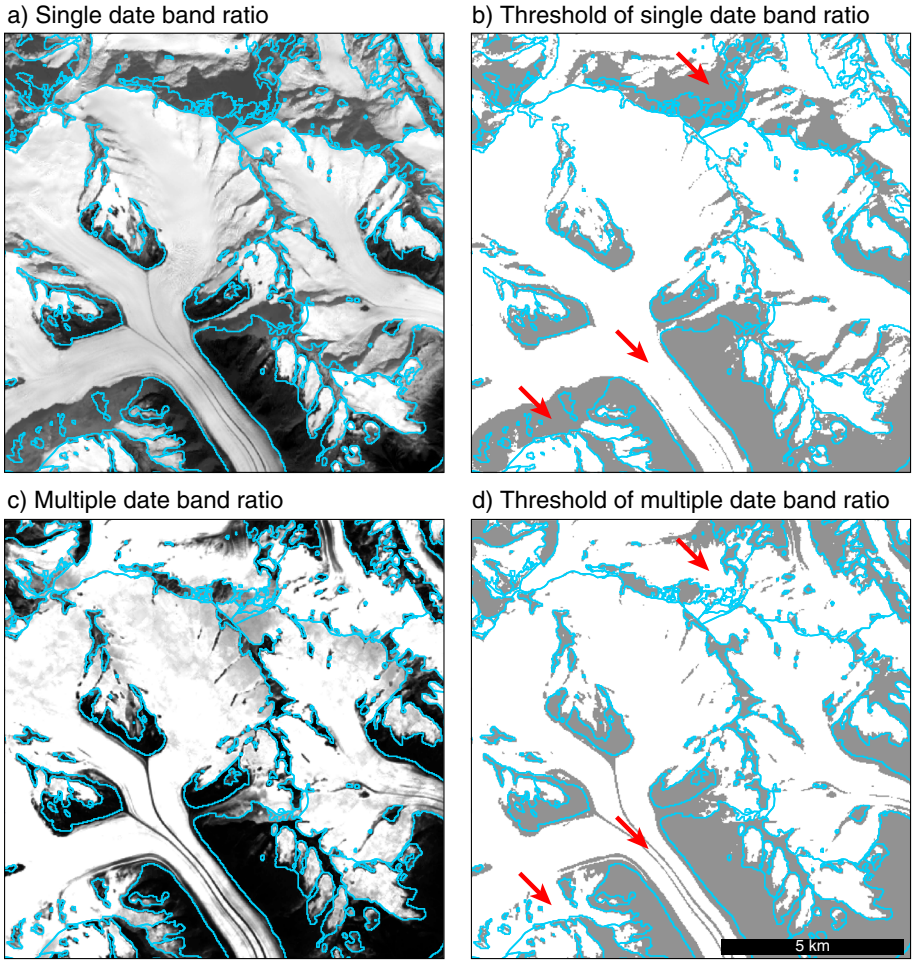

Figure 1. Debris-cover mapping from Landsat 8 (a and b) single date and (c and d) multiple date band ratio (band 4/band 6) images. Acquisition date of image in (a) and (b) is 3 October 2016. Threshold value used for (b) and (d) is 2.0. The arrows in (b) and (d) point at debris-free areas in shadows and debris-exposing medial moraines.

semiautomatically mapped supraglacial debris cover from the Karakoram and Pamir Mountains (Mölg et al., 2018). Second, we provide the first global assessment of the spatial distribution of supraglacial debris cover, excluding the Greenland ice sheet and Antarctica, which are mostly free of debris.

2. Materials and Methods

For mapping supraglacial debris cover, we combined an existing data set of glacier extents (including debris-covered portions) with remote sensing-based ice and snow identification. Glacier areas that are neither ice nor snow are classified as debris cover. This procedure has previously been used for mapping supraglacial debris cover (e.g., Herreid et al., 2015; Mölg et al., 2018), recently also with GEE (Kraaijenbrink et al., 2017). For glacier areas, we rely on the Randolph Glacier Inventory (RGI) version 6.0, which provides digital polygons of all glaciers on Earth, except for the Greenland and Antarctic ice sheets (RGI Consortium, 2017). Glacier outlines in the RGI have been both manually and automatically digitized, based primarily on optical satellite imagery but also on topographic maps (Pfeffer et al., 2014). Mapping of the debris-covered parts of glaciers is challenging due to the similar reflectance of debris compared to the surrounding terrain (e.g., Paul et al., 2004). Most regional glacier inventories that have been compiled in the RGI and that contain debris-covered glaciers thus rely, at least in part, on manual editing (e.g., Nuimura et al., 2015). In this study, we made no effort to change or modify the RGI outlines.

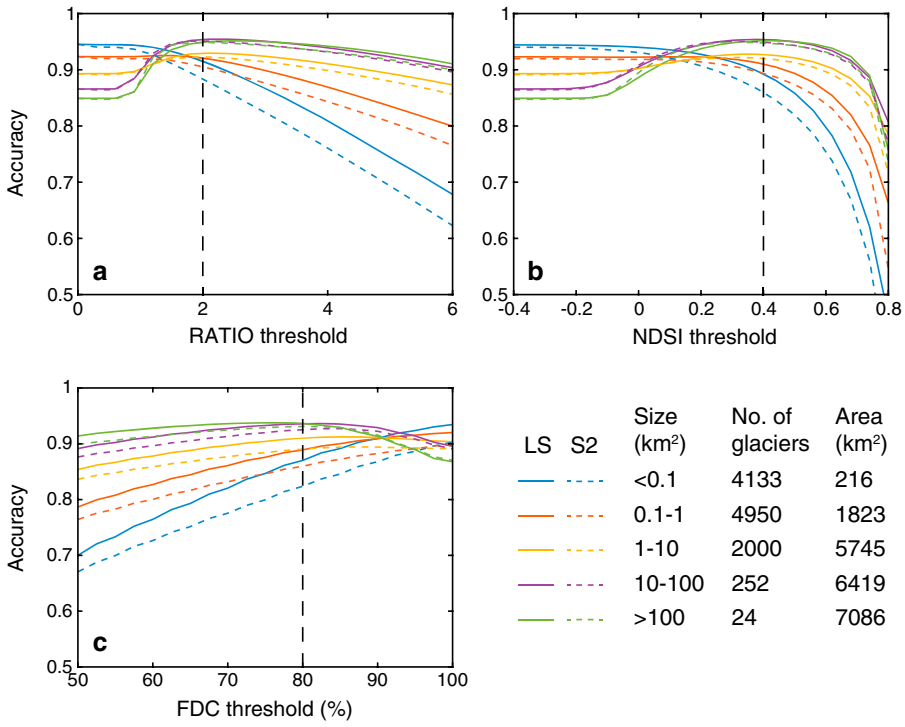

Figure 2. Sensitivity of ice and debris classification algorithms to the threshold values. The mapping accuracy is determined relative to the debris-cover classification of Mölg et al. (2018) and based on ~11,000 glaciers from the Karakoram. The vertical dashed lines indicate the threshold value used for the global mapping.

Figure S1 provides characteristics of the 19 geographic regions distinguished in the RGI (see the supporting information). In this study, we focused on optical satellite images from the time periods 2013–2017 (Landsat 8, 16-day repeat cycle at the equator) and 2015–2017 (Sentinel-2A/B, 5-day repeat cycle at the equator, when combined). In the case of Landsat 8, we restricted ourselves to images from the Tier-1 category, which are suitable for time series pixel-level analysis (https://landsat.usgs.gov/landsat-collections). We note that in some regions (e.g., New Zealand) the glacier outlines in the RGI are significantly older (Figure S1). Because glaciers are currently shrinking globally (Vaughan et al., 2013), such discrepancies are likely to result in overestimation of debris cover.

Common problems in ice-cover mapping from optical imagery are related to shadows as well as cloud and snow cover (Figures 1a and 1b; e.g., Winsvold et al., 2016). In manual approaches, the selection of suitable images is therefore an important but time-consuming first step (Paul et al., 2017). In our automatic approach, we tackled these problems by using a pixel-based instead of an image-based approach. This pixel-based approach makes use of all satellite images available during a given time period, which we subsequently filtered by (i) selecting only images from the melting season when snow cover is low and (ii) masking all images for cloud cover and cloud shadows. We define the melting season to comprise the days of year 200 to 300 (northern hemisphere) and 20 to 120 (southern hemisphere). We masked pixels in the images for cloud cover using a cloud score algorithm that also identifies associated cloud shadows based on the given solar geometry (Housman et al., 2018). In a last step, we computed for each pixel in each band a mean value from the 20th to 60th percentile range of the entire image stack to filter remaining clouds (bright pixels) and shadows (dark pixels; Figures 1c and 1d). Our procedure takes full advantage of the computational capacities of GEE as it enables us to process large amounts of satellite images in parallel.

The resulting image composites served as input for discriminating debris-free from debris-covered ice. We tested three different algorithms: a red to short-wavelength infrared (SWIR) band ratio (RATIO; Hall et al., 1987), the normalized difference snow index (NDSI; Dozier, 1989), and linear spectral unmixing-derived fractional debris cover (FDC; e.g., Keshava & Mustard, 2002). The RATIO ($\lambda_{red}/\lambda_{SWIR1}$) is based on Landsat 8 bands 4 (red) and 6 (SWIR1) and Sentinel-2 bands 4 (red) and 11 (SWIR1). The NDSI $[(\lambda_{green} - \lambda_{SWIR1})/(\lambda_{green} + \lambda_{SWIR1})]$

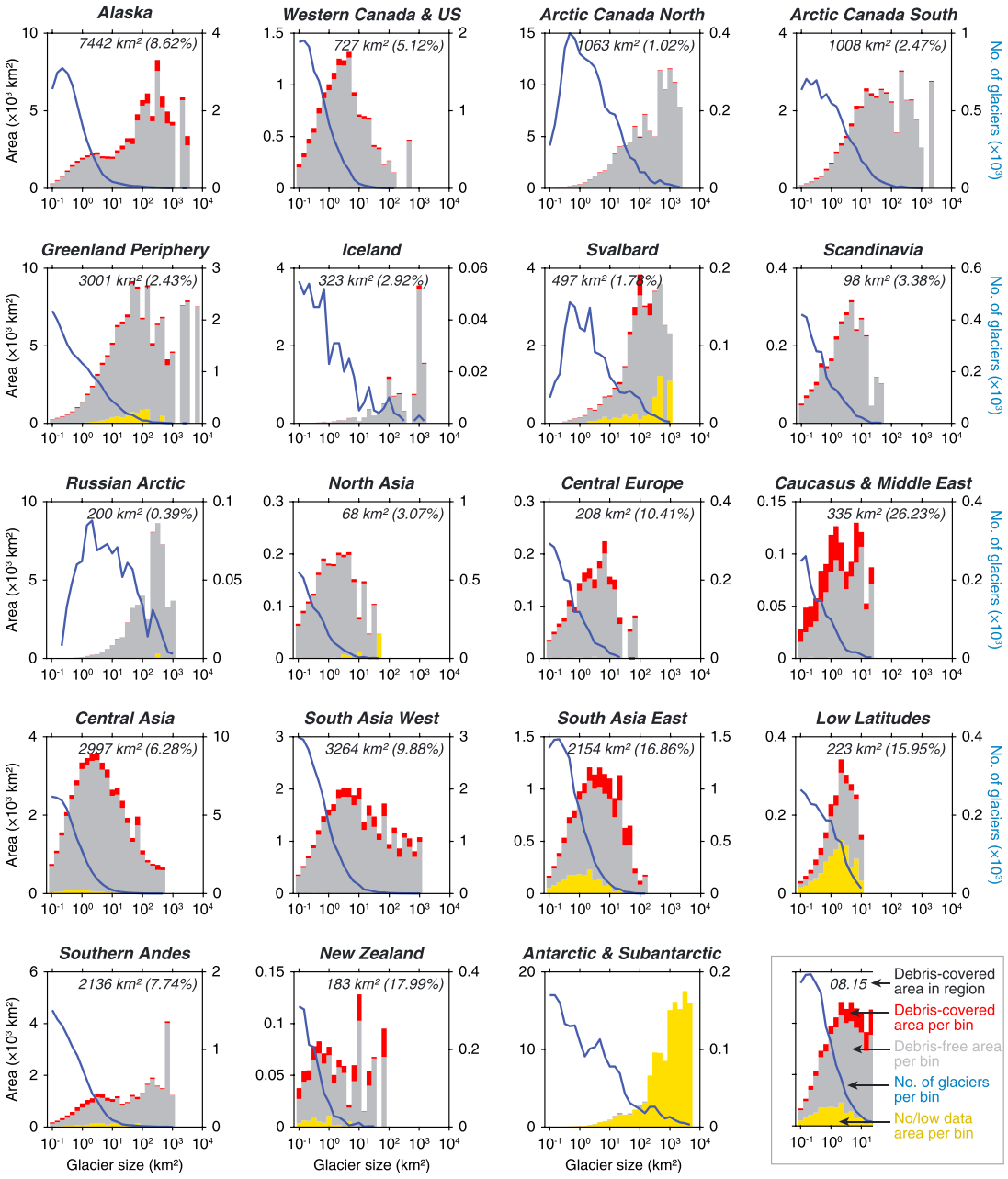

Figure 3. Distribution of debris cover by Randolph Glacier Inventory region and glacier size. In each region, the bars show glacier area per glacier size bin, indicating areas with debris (red), without debris (grey), and with no or low observations (COUNTS<10). The blue lines give glacier counts per bin. Text within axes gives total (relative) debris-covered area per region.

includes Landsat 8 bands 3 (green) and 6 (SWIR1) and Sentinel-2 bands 3 (green) and 11 (SWIR1). The basic principle of linear spectral unmixing is to decompose the measured spectrum of a pixel into a collection of end-members and a set of corresponding fractions that indicate the proportion of each end-member present in the pixel (Keshava & Mustard, 2002). To compute FDC, we used for each sensor the main spectral bands (Sentinel-2 bands: 2, 3, 4, 5, 6, 7, 8, 8a, 11, and 12; Landsat 8 bands: 2, 3, 4, 5, 6, and 7) and defined three end-member surface types for snow, ice, and debris, based on spectral ground measurements in the European Alps (Naegeli et al., 2017).

The outputs from GEE were four images for each sensor (Landsat 8 and Sentinel-2) with the same resolution as the input imagery; one each for RATIO, NDSI, and FDC and one image with the number of filtered

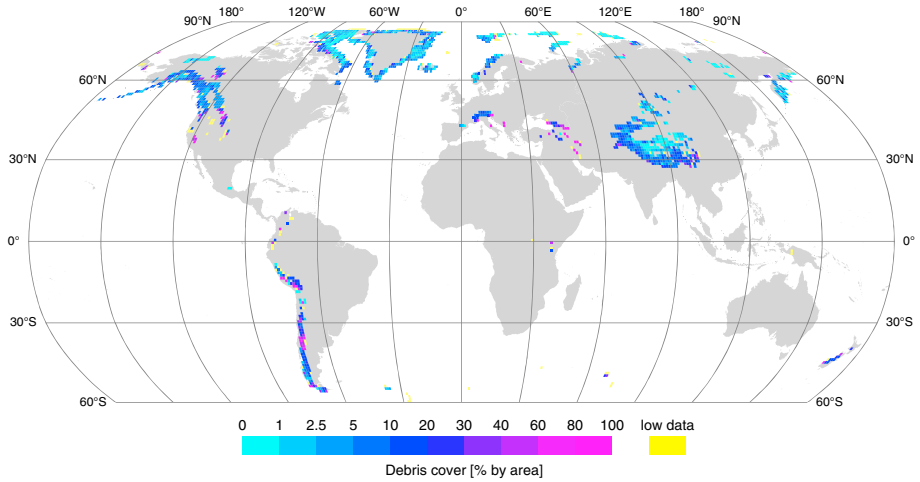

Figure 4. Global distribution of debris cover based on Landsat 8 imagery from the time period 2013–2015. Data are aggregated by area in 1 × 1 degree tiles. Low data correspond to areas where glaciers have no or low observations (COUNTS < 10) on average.

observations per pixel (COUNT). The number of observations is equal to the number of images available for the respective time period reduced by times when a pixel was masked as cloud or shadow. Because of the polar orbits of both Landsat 8 and Sentinel-2, mean COUNTS tend to increase poleward. However, glaciers in the Antarctic and Subantarctic have generally low COUNTS (Figure S2). In the case of Landsat 8, this may be attributed to lack of images in the Tier 1 category.

Finally, we defined debris-covered ice surfaces based on the RATIO, NDSI, and FDC images and threshold values of RATIO > 2.0 (e.g., Rastner et al., 2017), NDSI<0.4 (e.g., Dozier, 1989), and FDC > 80%. To find a suitable FDC threshold and to evaluate how sensitive the debris-cover classification is to the chosen threshold values, we compared a subset of our global data set with existing debris-cover maps from parts of South and Central Asia (Mölg et al., 2018), hereafter called the M2018 data set. The M2018 data set was created based on manually selected Landsat images acquired around the year 2000 (±2 years). Debris-cover extents were mapped manually in this study, using contrast-enhanced band composites and coherence images from ALOS1-PALSAR1 as a guide for identification (Mölg et al., 2018). We limited our comparison to ~11,000 glaciers whose outlines are identical in the RGI60 and M2018 data sets. These glaciers are situated in the Karakoram Mountains and have a wide range of sizes and debris-cover extents. We further restricted our comparison to areas situated below the median elevation of each glacier, because Mölg et al. (2018) eliminated any potential debris cover above it. We evaluated the debris-cover classification for different threshold values based on the accuracy, which we defined as the sum of true positive (debris cover in both data sets) and true negative (no debris cover in both data sets) image pixels divided by the total number of image pixels.

3. Results

3.1. Mapping Accuracy and Threshold Sensitivity

Compared to the M2018 data set, the mapping accuracy of our highly automated approach is mostly >0.9 for the RATIO and NDSI algorithms but lower for the FDC algorithm (Figure 2). For all three algorithms, we obtained higher accuracies for glaciers >10 km^2. For glaciers >1 km^2 the mapping accuracy is close to its maximum value and relatively insensitive to changes in the threshold value. For glaciers <1 km^2, however, the sensitivity is higher and the maximum mapping accuracy corresponds to threshold values that reduce the debris cover to a minimum. Furthermore, the mapping accuracies for all three algorithms are comparable between Landsat 8 and Sentinel-2 for glaciers >1 km^2, but the Sentinel-2 data set yields lower accuracies for glaciers <1 km^2. In summary, for glaciers <1 km^2 our automated mapping procedure yield systematically lower, but still acceptable, results compared to glaciers >1 km^2. However, because glaciers <1 km^2 account for <10% of the total ice-covered area, they do not have a large impact on our global assessment. Based on

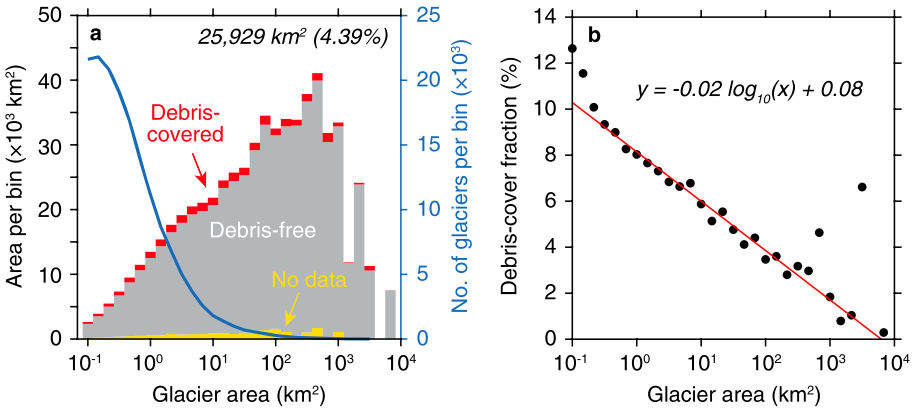

Figure 5. Global distribution of debris cover by glacier size (excluding Antarctica). (a) Glacier area (colored bars) and glacier counts (blue lines) per glacier area bin. (b) Areal fraction of debris cover per glacier size bin. Note that the equation yields debris-cover fraction between 0 and 1. Note that the number of glaciers $>10^3$ km^2 is only ~50.

the threshold values chosen for the global analysis, mapping accuracies are only slightly sensitive to the number of observations (COUNTS), although the Landsat 8 data set yields higher accuracies for COUNTS>10 (Figure S3).

3.2. Global Distribution of Debris Cover

Figure 3 shows the global distribution of debris cover distinguished by glacier size and RGI region, derived from the Landsat 8 data set and glaciers with >10 COUNTS on average (see Figure 4 for a global map of debris cover and Figure S4 for regional examples). The largest debris-covered areas are located in the RGI regions Alaska (7,442 km^2), followed by South Asia West (3,264 km^2) and Greenland Periphery (3,001 km^2). In relative terms, however, debris-covered glacier surfaces are most abundant in the Caucasus and Middle East (26.2%) followed by New Zealand (18%) and South Asia East (16.9%). At a global scale, ~26,000 km^2 of the studied glaciers are covered by debris, which equals ~4.4% by area (Figure 5a). When sorted by glacier area, the interquartile range (the middle 50%) of the entire debris-covered glacier area extends from glaciers that are ~3 to ~200 km^2 in area. Globally, the relative fraction of debris-covered areas systematically decreases with increasing glacier size (Figure 5b), but this pattern is not the same for all the RGI regions.

4. Discussion and Conclusions

Visual inspection of our results (e.g., Figure S4) and comparison with the M2018 data set from the Karakoram (Figure 2) shows that our automatic approach for debris-cover mapping using GEE produces robust results, from both Landsat 8 and Sentinel-2 imagery. We note that mismatches in the spatial distribution of debris cover between our and the M2018 data can also result from the temporal differences of the source imagery. The downglacier advection of looped medial moraines (e.g., Herreid & Truffer, 2016), for example, results in spatial distributions that change with time, although the debris-covered area may be constant. Furthermore, surging glaciers, which are particularly abundant in the Karakoram (e.g., Copland et al., 2011), can exhibit significant changes in both the distribution and extent of debris cover. Accounting for such uncertainties would most likely improve the correspondence between the two data sets. Hence, the pixel-based, multiple-date image fusion approach in GEE provides an efficient tool that allows for rapid and automated assessment of debris-cover extents.

The three main challenges we encountered for planetary-scale mapping of debris cover were (i) accurate glacier outlines, (ii) sufficient image coverage, and (iii) adequate algorithms and threshold values. First (i), inaccurate glacier outlines or mismatches between the time of glacier delineation and debris-cover mapping if the glacier has changed its extent (e.g., New Zealand; Figure S1) will unavoidably result in erroneous debris-cover maps (Figure S5). The latter point can be important for small glaciers (<1 km^2), where the relative rates of shrinkage are typically higher compared to larger glaciers (e.g., Narama et al., 2010). Second (ii), in some regions on Earth, we have insufficient image coverage to map debris cover. This is particularly true for

the RGI region Antarctic and Subantarctic (excluding the Antarctic ice sheet), where both Landsat 8 and Sentinel-2 imagery from our study period are scarce. Furthermore, our definition of the melting season appears suitable for the mid and high latitudes, but it may be less suitable for equatorial regions, where it could coincide with times of high cloud cover. This is likely the case in the RGI regions South Asia East and Low Latitudes (Figure 3). Third (iii), despite their simplicity, the RATIO and NDSI algorithms appear to yield robust results (e.g., Paul et al., 2002), which are better than those from the spectral unmixing approach (FDC). Although our sensitivity tests in the Karakoram support the chosen threshold values, this needs not be true for all regions on Earth. For example, detailed studies from the Alps have shown that the optimal NDSI thresholds can strongly vary in space and time and deviate from the commonly used value of 0.4 (Härer et al., 2018). Predicting such variations at a global scale is a remaining challenge. An alternative way to address this issue might be the use of a range of threshold values and assigning probabilities to debris cover.

The above challenges result in data gaps and misclassifications. Previous debris-cover mapping studies applied additional rules to minimize misclassifications that are, for example, based on the size or relative elevation of debris-cover patches (e.g., Herreid et al., 2015; Mölg et al., 2018). However, such approaches require a priori knowledge that we typically do not have. For example, debris in accumulation areas is either ephemeral or misclassified, because snow buries it quickly. If we knew the extent of accumulation areas exactly, we could eliminate misclassifications from them. However, accumulation areas estimated from the median elevation of a glacier (e.g., Mölg et al., 2018) are approximations that do not honor the fact that heavily debris-covered glaciers often have relatively larger ablation areas (e.g., Clark et al., 1994; Scherler et al., 2011), or that the boundary between accumulation and ablation area can vary in elevation spatially, even on a single glacier. Similarly, very small ($<$5 pixels) patches of debris often appear to result from inaccurate or outdated glacier outlines (e.g., Herreid et al., 2015), but this is not generally true. We therefore refrained from modifying the results from the automated debris-cover mapping in the first place and consider our results to most likely represent generous estimates. However, further improvements of the debris-cover maps may be possible by including and combining topographic (e.g., slope) and other spatial (e.g., relative elevation and proximity to edge) information of debris patches for identifying misclassifications.

Our global mapping has shown that RGI regions closer to the equator tend to have higher relative amounts of debris-covered areas compared to regions closer to the poles (Figures 3 and 4). This likely reflects the fact that glaciers near the equator are exclusively found in high mountain ranges that are typically steep and feature abundant steep rock walls, that is, the source areas of the debris. In regions that are closer to the poles, ice cover increases and topographic elevations decrease (Egholm et al., 2009)—to the extent that existing topography may even get buried by ice, hence eliminating any potential source areas for debris. The observed global scaling of debris-cover fraction with glacier size (Figure 5) supports the notion of source areas that get drowned with increasing glacier size. In consequence, we expect the areal fraction of debris cover to be lower during glacial periods, even in regions that currently feature abundant debris cover (e.g., Caucasus and Middle East; Figure 3), due to the much larger extent of glaciers. The Alpine ice sheet during the Last Glacial Maximum, for example, was covering most of the land surface (Mey et al., 2016), and in contrast to the present, the areal fraction of debris cover may have been smaller. On the other hand, smaller fractional areas together with much larger ice cover may still account for much larger absolute debris-covered areas, as presently in Alaska (Figure 3). Furthermore, if rates of debris supply to glaciers are influenced by temperature (e.g., Scherler, 2014), debris-cover extents may vary considerably with climatic changes. Therefore, the extent of supraglacial debris cover and its influence on glacial mass balances in mountainous regions should be accounted for in paleo-climatic reconstructions based on past glacial extents (e.g., Rowan et al., 2015). Finally, as glaciers continue to shrink, the influence of debris cover on glacier mass balances is expected to increase in the future.

Acknowledgments
This project has received funding from the European Research Council (ERC) under the European Union's Horizon 2020 research and innovation program under grant agreement 759639. Landsat 8 imagery provided by courtesy of the U.S. Geological Survey. Sentinel-2 imagery provided by courtesy of the EU Copernicus Program. Comments by two anonymous reviewers and discussions with F. Paul helped improve this paper. The debris-cover data sets are freely available from GFZ Data Services (Scherler et al., 2018) at http://doi.org/10.5880/GFZ.3.3.2018.005.

References

Clark, D. H., Clark, M. M., & Gillespie, A. R. (1994). Debris-covered glaciers in the Sierra Nevada, California, and their implications for snowline reconstructions. *Quaternary Research*, *41*(02), 139–153. https://doi.org/10.1006/qres.1994.1016

Copland, L., Sylvestre, T., Bishop, M. P., Shroder, J. F., Seong, Y. B., Owen, L. A., Bush, A., et al. (2011). Expanded and recently increased glacier surging in the Karakoram. *Arctic, Antarctic, and Alpine Research*, *43*(4), 503–516. https://doi.org/10.1657/1938-4246-43.4.503

Deline, P. (2005). Change in surface debris cover on Mont Blanc massif glaciers after the 'Little Ice Age' termination. *The Holocene*, *15*(2), 302–309. https://doi.org/10.1191/0959683605hl809rr

Dozier, J. (1989). Spectral signature of alpine snow cover from the Landsat Thematic Mapper. *Remote Sensing of Environment*, *28*, 9–22. https://doi.org/10.1016/0034-4257(89)90101-6

Egholm, D. L., Nielsen, S. B., Pedersen, V. K., & Lesemann, J.-E. (2009). Glacial effects limiting mountain height. *Nature Geoscience*, *460*(7257), 884–887. https://doi.org/10.1038/nature08263

Gorelick, N., Hancher, M., Dixon, M., Ilyushchenko, S., Thau, D., & Moore, R. (2017). Google Earth Engine: Planetary-scale geospatial analysis for everyone. *Remote Sensing of Environment*, *202*, 18–27. https://doi.org/10.1016/j.rse.2017.06.031

Hall, D. K., Ormsby, J. P., Bindschadler, R. A., & Siddalingaiah, H. (1987). Characterization of snow and ice reflectance zones on glaciers using Landsat Thematic Mapper data. *Annals of Glaciology*, *9*, 104–108. https://doi.org/10.3189/S0260305500000471

Härer, S., Bernhardt, M., Siebers, M., & Schulz, K. (2018). On the need for a time- and location-dependent estimation of the NDSI threshold value for reducing existing uncertainties in snow cover maps at different scales. *The Cryosphere*, *12*(5), 1629–1642. https://doi.org/10.5194/tc-12-1629-2018

Herreid, S., Pellicciotti, F., Ayala, A., Chesnokova, A., Kienholz, C., Shea, J., & Shrestha, A. (2015). Satellite observations show no net change in the percentage of supraglacial debris-covered area in northern Pakistan from 1977 to 2014. *Journal of Glaciology*, *61*(227), 524–536. https://doi.org/10.3189/2015JoG14J227

Herreid, S., & Truffer, M. (2016). Automated detection of unstable glacier flow and a spectrum of speedup behavior in the Alaska Range. *Journal of Geophysical Research: Earth Surface*, *121*, 64–81. https://doi.org/10.1002/2015JF003502

Housman, I. W., Chastain, R. A., & Finco, M. V. (2018). An evaluation of forest health insect and disease survey data and satellite-based remote sensing forest change detection methods: Case studies in the United States. *Remote Sensing*, *10*(8), 1184. https://doi.org/10.3390/rs10081184

Huss, M., & Hock, R. (2015). A new model for global glacier change and sea-level rise. *Frontiers in Earth Science*, *3*, 54. https://doi.org/10.3389/feart.2015.00054

Huss, M., & Hock, R. (2018). Global-scale hydrological response to future glacier mass loss. *Nature Climate Change*, *8*(2), 135–140. https://doi.org/10.1038/s41558-017-0049-x

Keshava, N., & Mustard, J. F. (2002). Spectral unmixing. *IEEE Signal Processing Magazine*, *19*(1), 44–57. https://doi.org/10.1109/79.974727

Kirkbride, M. P., & Deline, P. (2013). The formation of supraglacial debris covers by primary dispersal from transverse englacial debris bands. *Earth Surface Processes and Landforms*, *38*(15), 1779–1792. https://doi.org/10.1002/esp.3416

Kraaijenbrink, P. D. A., Bierkens, M. F. P., Lutz, A. F., & Immerzeel, W. W. (2017). Impact of a global temperature rise of 1.5 degrees Celsius on Asia's glaciers. *Nature*, *549*(7671), 257–260. https://doi.org/10.1038/nature23878

Marzeion, B., Jarosch, A. H., & Hofer, M. (2012). Past and future sea-level change from the surface mass balance of glaciers. *The Cryosphere*, *6*(6), 1295–1322. https://doi.org/10.5194/tc-6-1295-2012

Mey, J., Scherler, D., Wickert, A. D., Egholm, D. L., Tesauro, M., Schildgen, T. F., & Strecker, M. R. (2016). Glacial isostatic uplift of the European Alps. *Nature Communications*, *7*, 13382. https://doi.org/10.1038/ncomms13382

Mölg, N., Bolch, T., Rastner, P., Strozzi, T., & Paul, F. (2018). A consistent glacier inventory for the Karakoram and Pamir regions derived from Landsat data: Distribution of debris cover and mapping challenges. *Earth System Science Data*, *10*(4), 1807–1827. https://doi.org/10.5194/essd-10-1807-2018

Naegeli, K., Damm, A., Huss, M., Wulf, H., Schaepman, M., & Hoelzle, M. (2017). Cross-comparison of albedo products for glacier surfaces derived from airborne and satellite (Sentinel-2 and Landsat 8) optical data. *Remote Sensing*, *9*(2), 110. https://doi.org/10.3390/rs9020110

Narama, C., Kääb, A., Duishonakunov, M., & Abdrakhmatov, K. (2010). Spatial variability of recent glacier area changes in the Tien Shan Mountains, Central Asia, using Corona (~1970), Landsat (~2000), and ALOS (~2007) satellite data. *Global and Planetary Change*, *71*(1-2), 42–54. https://doi.org/10.1016/j.gloplacha.2009.08.002

Nuimura, T., Sakai, A., Taniguchi, K., Nagai, H., Lamsal, D., Tsutaki, S., Kozawa, A., et al. (2015). The GAMDAM glacier inventory: A quality-controlled inventory of Asian glaciers. *The Cryosphere*, *9*(3), 849–864. https://doi.org/10.5194/tc-9-849-2015

Østrem, G. (1959). Ice melting under a thin layer of moraine, and the existence of ice cores in moraine ridges. *Geografiska Annaler*, *41*(4), 228–230. https://doi.org/10.1080/20014422.1959.11907953

Paul, F., Huggel, C., & Kääb, A. (2004). Combining satellite multispectral image data and a digital elevation model for mapping debris-covered glaciers. *Remote Sensing of Environment*, *89*(4), 510–518. https://doi.org/10.1016/j.rse.2003.11.007

Paul, F., Kääb, A., Maisch, M., Kellenberger, T., & Haeberli, W. (2002). The new remote-sensing-derived Swiss glacier inventory: I. Methods. *Annals of Glaciology*, *34*, 355–361. https://doi.org/10.3189/172756402781817473

Paul, F., Bolch, T., Briggs, K., Kääb, A., McMillan, M., McNabb, R., et al. (2017). Error sources and guidelines for quality assessment of glacier area, elevation change, and velocity products derived from satellite data in the Glaciers_cci project. *Remote Sensing of Environment*, *203*, 256–275. https://doi.org/10.1016/j.rse.2017.08.038

Pfeffer, W. T., Arendt, A. A., Bliss, A., Bolch, T., Cogley, J. G., Gardner, A. S., Hagen, J. O., et al., & The Randolph Consortium (2014). The Randolph Glacier Inventory: A globally complete inventory of glaciers. *Journal of Glaciology*, *60*(221), 537–552. https://doi.org/10.3189/2014JoG13J176

Rastner, P., Strozzi, T., & Paul, F. (2017). Fusion of multi-source satellite data and DEMs to create a new glacier inventory for Novaya Zemlya. *Remote Sensing*, *9*(11), 1122. https://doi.org/10.3390/rs9111122

RGI Consortium (2017). Randolph Glacier Inventory (RGI)—A dataset of global glacier outlines: Version 6.0, Technical Report, Global Land Ice Measurements from Space, Boulder, Colorado, USA, Digital Media. https://doi.org/10.7265/N5-RGI-60

Rowan, A. V., Egholm, D. L., Quincey, D. J., & Glasser, N. F. (2015). Modelling the feedbacks between mass balance, ice flow and debris transport to predict the response to climate change of debris-covered glaciers in the Himalaya. *Earth and Planetary Science Letters*, *430*, 427–438. https://doi.org/10.1016/j.epsl.2015.09.004

Scherler, D. (2014). Climatic limits to headwall retreat in the Khumbu Himalaya, eastern Nepal. *Geology*, *42*(11), 1019–1022. https://doi.org/10.1130/G35975.1

Scherler, D., Bookhagen, B., & Strecker, M. R. (2011). Hillslope-glacier coupling: The interplay of topography and glacial dynamics in High Asia. *Journal of Geophysical Research*, *116*, F02019. https://doi.org/10.1029/2010JF001751

Scherler, D., Wulf, H., & Gorelick, N. (2018). Supraglacial debris cover. V. 1.0. GFZ German Research Centre for Geosciences. https://doi.org/10.5880/GFZ.3.3.2018.005

Vaughan, D. G., Comiso, J. C., Allison, I., Carrasco, J., Kaser, G., Kwok, R., Mote, P., et al. (2013). Observations: Cryosphere. In T. F. Stocker, et al. (Eds.), *Climate change 2013: The physical science basis. Contribution of Working Group I to the Fifth Assessment Report of the Intergovernmental Panel on Climate Change* (Chap. 4, pp. 317–382). Cambridge, UK and New York: Cambridge University Press.

Winsvold, S. H., Kääb, A., & Nuth, C. (2016). Regional glacier mapping using optical satellite data time series. *IEEE Journal of Selected Topics in Applied Earth Observations and Remote Sensing*, *9*(8), 3698–3711. https://doi.org/10.1109/JSTARS.2016.2527063